Antiproliferative novel isoxazoles: Modeling, virtual screening, synthesis, and bioactivity evaluation

ARTICLE *in* EUROPEAN JOURNAL OF MEDICINAL CHEMISTRY · MAY 2014

Impact Factor: 3.45 · DOI: 10.1016/j.ejmech.2014.05.011 · Source: PubMed

7 AUTHORS, INCLUDING:

Sandra Liekens
University of Leuven
93 PUBLICATIONS **1,946** CITATIONS
SEE PROFILE

Georgia Melagraki
50 PUBLICATIONS **967** CITATIONS
SEE PROFILE

Antreas Afantitis
49 PUBLICATIONS **952** CITATIONS
SEE PROFILE

Nikolas Fokialakis
National and Kapodistrian University of Ath…
91 PUBLICATIONS **663** CITATIONS
SEE PROFILE

European Journal of Medicinal Chemistry 81 (2014) 139–149

Contents lists available at ScienceDirect

European Journal of Medicinal Chemistry

journal homepage: http://www.elsevier.com/locate/ejmech

Original article

Antiproliferative novel isoxazoles: Modeling, virtual screening, synthesis, and bioactivity evaluation

Evangelia Tzanetou [a], Sandra Liekens [b], Konstantinos M. Kasiotis [c], Georgia Melagraki [d], Antreas Afantitis [d], Nikolas Fokialakis [e], Serkos A. Haroutounian [a,*]

[a] Agricultural University of Athens, Chemistry Laboratory, Iera Odos 75, Athens 11855, Greece
[b] Rega Institute for Medical Research, KU Leuven, Minderbroedersstraat 10, B-3000 Leuven, Belgium
[c] Benaki Phytopathological Institute, Laboratory of Pesticides Toxicology, 8 St. Delta Street, Athens, Kifissia 14561, Greece
[d] Department of Chemoinformatics, NovaMechanics Ltd, John Kennedy Ave 62-64, Nicosia 1046, Cyprus
[e] Department of Pharmacognosy and Natural Products Chemistry, Faculty of Pharmacy, University of Athens, Panepistimiopolis, Zografou 15771, Athens, Greece

ARTICLE INFO

Article history:
Received 10 January 2014
Received in revised form
16 March 2014
Accepted 2 May 2014
Available online 4 May 2014

Keywords:
Isoxazoles
Chemical synthesis
Classification model
Virtual screening
Antiproliferative activity
In silico

ABSTRACT

A series of novel isoxazole derivatives were efficiently synthesized through the adaptation/modification of an *in situ* synthetic procedure for pyrazoles. All novel compounds were tested against four different cell lines to evaluate their antiproliferative activity. Based on the Hela cells results of this study and previous work, a classification model to predict the anti-proliferative activity of isoxazole and pyrazole derivatives was developed. Random Forest modeling was used in view of the development of an accurate and reliable model that was subsequently validated. A virtual screening study was then proposed for the design of novel active derivatives. Compounds **9** and **11** demonstrated significant cytostatic activity; the fused isoxazole derivative **18** and the virtually proposed compound **2v**, were proved at least 10 times more potent as compared to compound **9**, with IC50 values near and below 1 μM. In conclusion, a new series of isoxazoles was exploited with some of them exhibiting promising cytostatic activities. Further studies on the substitution pattern of the isoxazole core can potentially provide compounds with cytostatic action at the nM scale. In this direction the *in silico* approach described herein can also be used to screen existing databases to identify derivatives with anticipated activity.

1. Introduction

Cancer is considered as one of the most multifactorial diseases of the world resulting from a combined influence of genetic and environmental factors and involving a multitude of cells, receptors, soluble factors and extracellular matrix molecules. As such, cancer requires multifactorial treatment, targeting different cell types and/or signaling pathways [1,2] Consequently, a considerable focus has recently been devoted to the discovery and development of new, more selective anticancer agents [3,4] that are capable to intervene with these pathways.

Among the diverse azaheterocyclic ring systems considered as potent antitumor agents, the isoxazole core structure constitutes one of the most promising five-membered heterocyclic systems [5,6]. In particular, several resorcinolic isoxazole amides, exemplified by the molecule of NVP-AUY922 (Fig. 1) have been determined as very potent inhibitors of heat shock proteins (HSP90) [7–9]. The molecule of NVP-AUY922 inhibits the human tumor cell proliferation and migration, displaying significant anti-angiogenic properties, as was established for the inhibition of tube formation of human endothelial cells and the reduction of microvessels density in various tumor xenografts [7]. Thus, this compound is under Phase II clinical trials for several years [8].

In this view, a considerable research effort has been initiated towards the thorough investigation of the antitumor properties of compounds containing the isoxazole residue. Indicatively and aiming to enhance their antitumor properties, various isoxazole derivatives have been conjugated with pharmacophore benzodiazepines [10], while a 3,5-diaryl isoxazole derivative was assessed to display high affinity for the retinoic acid receptor (RAR) combined with selective apoptosis-inducing activity [11].

In the course of our longstanding research interest concerning the development of bioactive azaheterocycles ([12,13]), we have relied on the abovementioned data for the design, synthesis and

* Corresponding author. Agricultural University of Athens, Department of Sciences, Chemistry Laboratory, Iera Odos 75, Athens 11855, Greece.
E-mail address: sehar@aua.gr (S.A. Haroutounian).

http://dx.doi.org/10.1016/j.ejmech.2014.05.011
0223-5234/

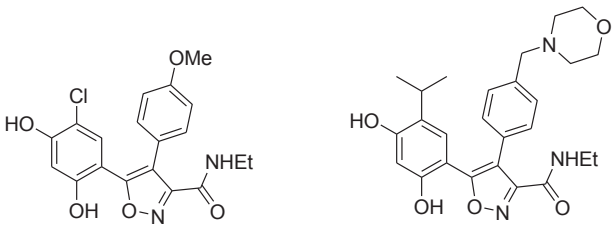

Fig. 1. Chemical structures of resorcinylic isoxazoles VER-50589 and NVP-AUY922.

bioactivity assessment of a series of novel compounds containing in their structural framework a fused isoxazole residue. The latter was efficiently approached through the developed and adapted herein one pot addition of hydroxylamine to tetralone and acetophenone substrates. The anti-proliferative activities of the novel compounds were evaluated against a panel of two tumor and two endothelial cell lines and the respective results were elaborated into *in silico* modeling. The latter is emerged as a useful tool for the identification of new leads with improved characteristics [14–16], via the employment of different modeling methods which minimize the time and cost associated with their identification. In this context, a classification model was developed that combines the isoxazole and pyrazole structures with their antiproliferative activity. The virtual screening model development was based on the inhibition of Hela cells. The model was fully validated and proven robust and accurate. Therefore was utilized to virtually explore novel structures and succeeded in identifying novel potent inhibitors that were experimentally validated.

2. Results and discussion

2.1. Synthesis

The reported to date methods of constructing the isoxazole structural framework refer to the following reactions: i) cycloaddition of alkenes/alkynes to nitrile oxides, ii) addition of hydroxylamine to 1,3-diketones, 1,3-dialkynes or α,β-unsaturated ketones, aldehydes or nitriles, iii) cyclization of alkynyl oxime ethers, and iv) palladium-catalyzed four-component coupling, as reported in 2005 [17].

In this work, good to excellent yields of the target isoxazoles were obtained through the adaptation/modification of a methodology published in 2006 for the *in situ* synthesis of pyrazoles by addition of hydrazines to 1,3-diketones [18]. This method proceeds via a similar mechanistic pattern as the one pot addition of hydroxylamine to various 1,3-diketones, constituting a fast and efficient synthetic route for constructing various isoxazoles and/or the synthetically challenging isoxazole-containing fused rings.

More specifically, in the presence of lithium hexamethyl disilazane (LHMDS) and anhydrous conditions the easily accessible acetophenone **1**–**4** substrates were converted to the corresponding anions, which were subsequently condensed with the 4-methoxyanisoyl chloride to yield the 3-diketone derivatives (Scheme 1). Consecutively, the latter was *in situ* condensed with hydroxylamine to provide in one overall step the desired isoxazole structures (compounds **5**–**8**, 64–80% total yields). Deprotection of the latter with boron tribromide (BBr_3) at −78 °C provided the isoxazoles **9**–**12**. Accordingly, the reaction of tetralones **13** and **14** with various benzoyl chlorides resulted in good yields (49–67%) of the isoxazole-tetralone fused ring system-containing compounds **15**–**18**, **21** and **23** (Schemes 2 and 3). Compounds **16**, **18** and **21** were also deprotected in almost quantitative yields by reaction with BBr_3 providing the target derivatives **19**, **20** and **22**.

The structure of the synthesized isoxazoles was elucidated using several 2D-NMR methods, such as the COSY, HSQC and HMBC experiments. In particular, the configuration of compounds **5**–**12** was assigned through the long range correlation of C-5 (downfield > 166 ppm) with H-6′ and H-2′, which is characteristic for all similar compounds and indicative of the proposed structures. Similarly, the correlation between C-5 and H-7 and H-13 in the HMBC experiment for isoxazoles **15**–**23** was used for the unambiguous assignment of the synthesized compounds (see supporting information).

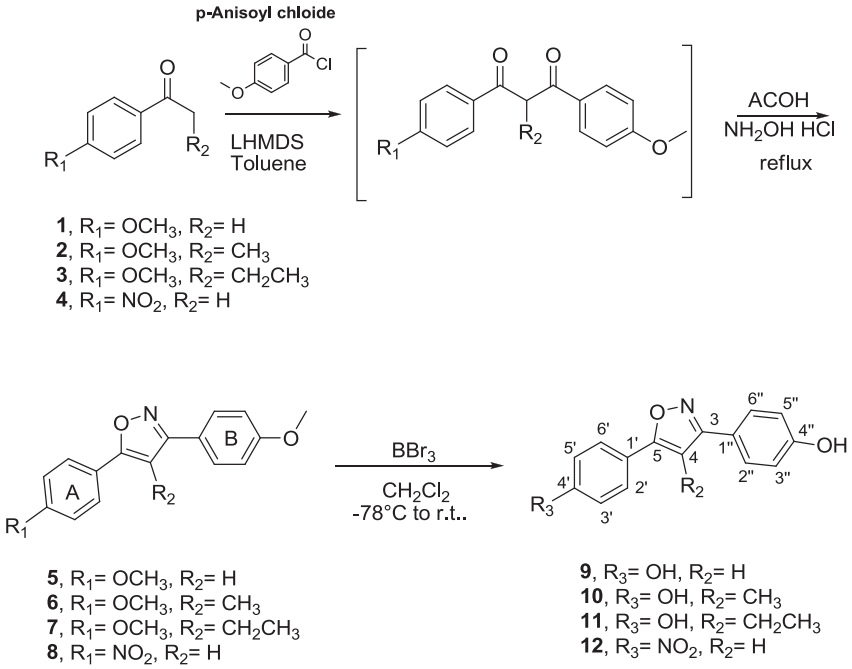

Scheme 1. One pot approach of isoxazoles from acetophenones substrates.

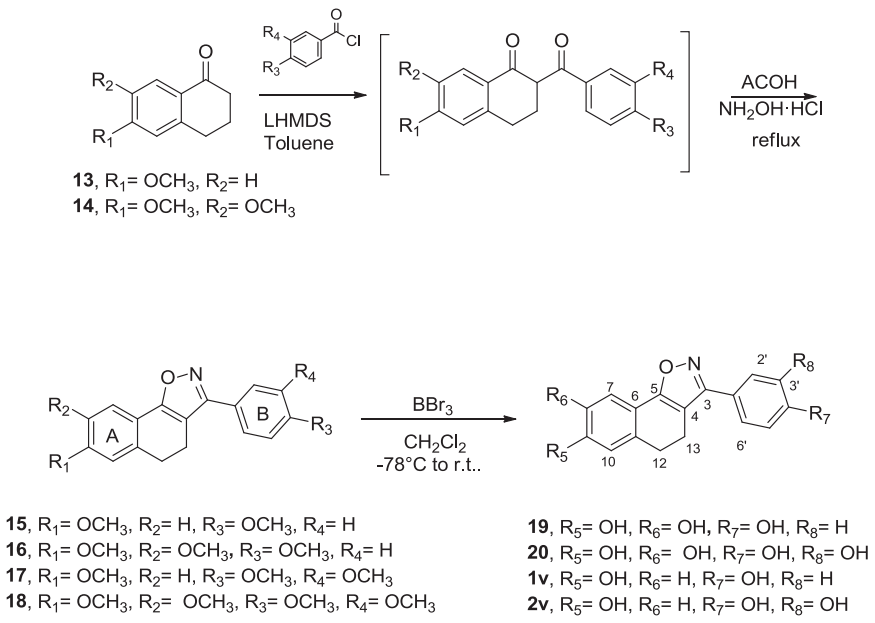

13, R_1= OCH_3, R_2= H
14, R_1= OCH_3, R_2= OCH_3

15, R_1= OCH_3, R_2= H, R_3= OCH_3, R_4= H
16, R_1= OCH_3, R_2= OCH_3, R_3= OCH_3, R_4= H
17, R_1= OCH_3, R_2= H, R_3= OCH_3, R_4= OCH_3
18, R_1= OCH_3, R_2= OCH_3, R_3= OCH_3, R_4= OCH_3

19, R_5= OH, R_6= OH, R_7= OH, R_8= H
20, R_5= OH, R_6= OH, R_7= OH, R_8= OH
1v, R_5= OH, R_6= H, R_7= OH, R_8= H
2v, R_5= OH, R_6= H, R_7= OH, R_8= OH

Scheme 2. Synthesis of tetralone-isoxazole fused ring systems.

2.2. Anti-proliferative properties of the isoxazole derivatives

The anti-proliferative activity of the novel isoxazoles **5**–**12** and **15**–**23** was evaluated in four different cell lines: two endothelial cell lines [human microvascular endothelial cells (HMEC-1) and mouse brain endothelial cells (MBEC)] and two tumor cell lines [human cervical carcinoma (HeLa) and human breast carcinoma (MCF-7) cells]. Data are expressed as IC_{50} (50% inhibitory concentration), defined as the compound concentration that reduces cell proliferation by 50%, and are shown in Table 1.

Among the flexible analogues (**5**–**12**) compounds **5**–**8**, containing an *o*-CH_3 or NO_2 at R_1 showed no anti-proliferative activity in any of the cell lines tested (IC_{50} > 100 μM). However, the replacement of the *o*-CH_3 by an OH resulted in a significant

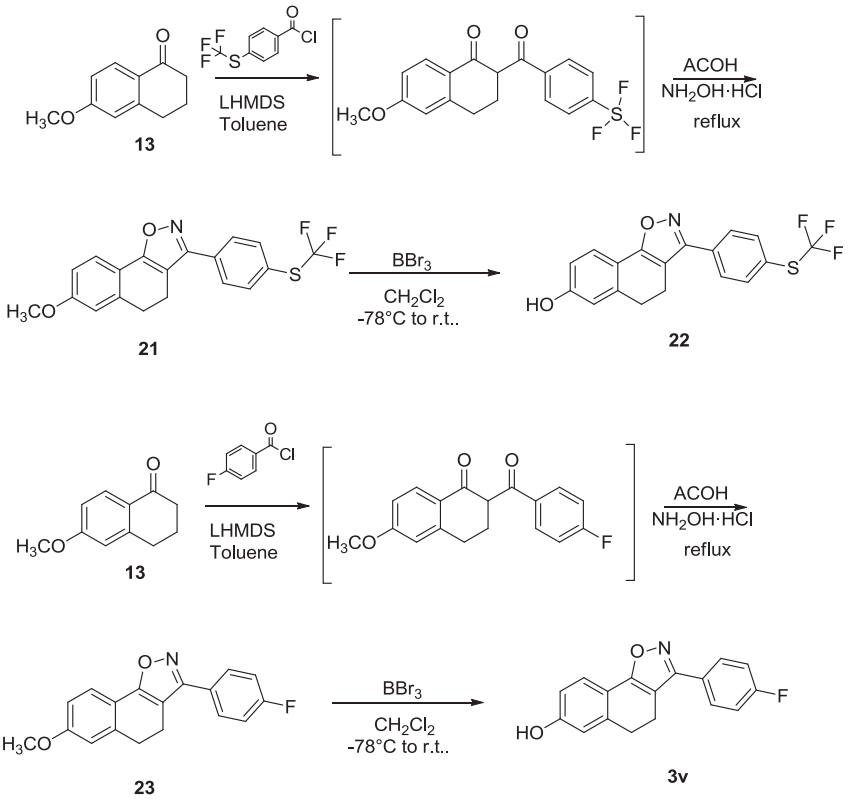

13
21
22
13
23
3v

Scheme 3. Synthesis of substituted fused tetralone-isoxazole derivatives.

Table 1
Antiproliferative activities of novel isoxazoles.

Compound	IC50 (μM)			
	HMEC-1	MBEC	HeLa	MCF-7
5	>100	>100	>100	>100
6	>100	>100	>100	>100
7	>100	>100	>100	>100
8	>100	>100	>100	>100
9	6.3 ± 0.5	2.5 ± 0.2	6 ± 0.9	5.2 ± 0.3
10	47 ± 1	19 ± 3	15 ± 3	48 ± 2
11	9.7 ± 1.1	13 ± 2	16 ± 1	9.8 ± 0.4
12	27 ± 7	42 ± 1	57 ± 6	53 ± 2
15	>100	>100	>100	>100
16	>100	>100	>100	>100
17	>100	>100	>100	>100
18	0.56 ± 0.12	1.1 ± 0.1	0.59 ± 0.08	0.36 ± 0.05
19	7.4 ± 0.8	6.8 ± 0.1	10 ± 1	2.1 ± 0.1
20	4.2 ± 2.2	10 ± 1	9.1 ± 0.6	2.1 ± 0.1
21	>100	>100	>100	>100
22	65 ± 20	67 ± 20	55 ± 36	81 ± 19
23	>100	>100	34 ± 15	>100

improvement of their activity. In particular, compounds **9** and **11**, without substituent or an ethyl at R_2, respectively, demonstrated a significant cytostatic activity in endothelial and tumor cell lines with IC_{50} values ranging from 2.5 to 6 μM for **9** and 9.7 to 16 μM for **11**. Derivative **10**, holding a methyl group at R_2 showed comparable activity as **11** in MBEC and HeLa cells, but proved to be 5-fold less potent in HMEC-1 and MCF-7 cells. Compound **12** (containing a NO_2 at R_3 and no substituent at R_2) showed only moderate cytostatic activity with IC_{50} values between 27 and 57 μM. Thus, among this series of compounds, an OH at R_3 and no substituent at R_2 are preferred, affording anti-proliferative activity in endothelial and tumor cell lines in the lower micromolar range.

Next, the fused tetralone-isoxazole derivatives were evaluated for their anti-proliferative activity. Similar to the flexible compounds described above, compounds **15**–**17** with an *o*-CH_3 at R_1 were inactive, regardless of whether they contained one or two additional *o*-CH_3 at R_2, R_3 and/or R_4. However, **18** containing methoxy groups at R_1, R_2, R_3 and R_4 proved 10-fold more active than the best flexible compound **9**, with IC_{50} values between 0.36 and 1.1 μM, depending on the cell line. Demethylation of compounds **16** and **18** provided isoxazoles **19**–**20**, with cytostatic activity in the lower micromolar range. Notably, compound **20** was 10-fold less active than **18**.

The substituted derivatives **21**–**23** displayed only moderate (IC_{50} of 34–81 μM for the deprotected compounds) or no anti-proliferative activity.

2.3. In silico exploration

In an effort to develop a method for the design and identification of novel compounds with improved antiprofilerative activity, a series of 33 novel inhibitors of Hela cell proliferation, mainly isoxazole and pyrazole derivatives, were analyzed computationally. The dataset contains the compounds described in this work (compounds **5**–**12**, **15**–**23**) combined with sixteen pyrazoles that have been previously explored as anti-proliferative agents [13] (Fig. 2).

For preprocessing, cleansing, attribute selection, modeling and validation of our data we have created a KNIME workflow suitable to run step by step all the computational tasks essential for the development of a validated model [19]. In particular, we have created a KNIME workflow that implements the development of a predictive model following the sequence described as following: Compounds and inhibition data were imported and pre-processed, descriptors were calculated and selected, the Random Forest algorithm was implemented, the produced model was validated and the domain of applicability was defined.

The original dataset of the 33 inhibitors of the Hela cells was randomly partitioned into training and validation set in a ratio of 70:30 consisting of 24 and 9 compounds respectively. The training set was used to develop the QSAR models as described below whereas the test set was not involved by any means in the model development. For each compound 294 descriptors were calculated using the Chemistry Development Kit (CDK) [20], which account for the topological, geometric and structural characteristics of compounds. As some of the descriptors do not have any discrimination power (i.e. they have no variation) a filter was applied for their removal. In total 159 descriptors remained to be used as possible inputs during the QSAR model development.

The CfsSubset variable selection with BestFirst evaluator method was then applied on the training data to select the most significant, among the 159 available descriptors. Four descriptors were selected as the most important for the development of the model. The selected descriptors are BCUTp-1l, Wlambda3unity, Wnu2unity and Weta1unity.

BCUT molecular descriptor is an eigenvalue based descriptor that has been shown to be useful in chemical diversity metrics and have enabled implementation of cell-based algorithms for diversity-related tasks [21]. BCUT is based on a weighted version of the Burden matrix which takes into account both the connectivity as well as atomic properties of a molecule [22]. BCUTp-1l corresponds to lowest atomic related polarizability weighted value.

Wlambda3unity, Wnu2unity and Weta1unity belong to the Weighted Holistic Invariant Molecular descriptors (WHIM descriptors) which are based on statistical indices calculated on the projections of the atoms along principal axes [23]. WHIM descriptors encode information relevant to 3D molecular structure, size, shape, symmetry and atom distribution with respect to invariant frames [24].

The training set contains 24 compounds (15 “actives” and 9 “inactive”) and the test set 9 compounds (5 “actives” and 4 “inactive”). The cutoff value for the discrimination between “actives” and “inactives” was set to $IC_{50} > 100$ μM.

A classification model has been developed in order to separate active from inactive compounds and filter out the inactive ones. Random Forest (RF) classification technique with 15 trees, implemented in the WEKA program [25], was used to discriminate between the different classes.

After the classification model was trained, prediction on the activity of test compounds was performed. The experimental values and the predictions for both training and test examples are presented in Table 2. The confusion matrix for the cross validation method and model predictions on the external test set, are presented in Tables 3 and 4. The performance of the model was evaluated based on validation measurements described before. The significance, accuracy and robustness of the model are illustrated by the corresponding statistics (see Table 5). In particular, the application of the 10-fold cross validation method produced the following statistics: precision = 92.9%, sensitivity = 86.725%, specificity = 88.9% and accuracy = 87.5%. By applying the model to the external test set, the following statistical results were obtained: precision = 100%, sensitivity = 83.3%, specificity = 100% and accuracy = 89%.

The applicability domain was defined for all compounds that constituted the test sets as described in the Materials and Methods section. Since all validation compounds fell inside the domain of applicability, all model predictions for the external test set were considered reliable except for compound P1 (APD limit 1.76).

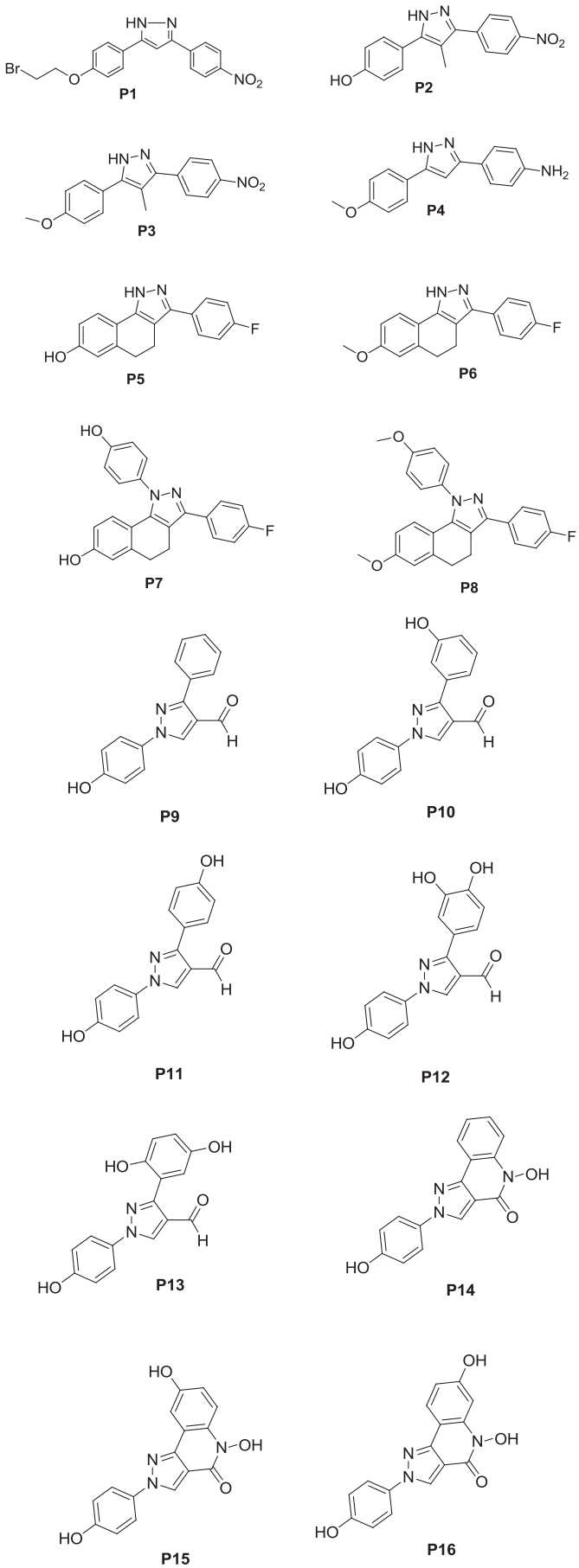

2.4. In silico virtual screening

The proposed method, due to the high predictive ability and simplicity [26–28] can be considered as a useful aid to the costly and time-consuming experiments for the synthesis and the determination of inhibition of the human cervical carcinoma (Hela) cells by isoxazole and pyrazole derivatives. The design of novel active molecules by the insertion, deletion, or modification of substituents on different sites of the molecule and at different positions could therefore be guided by the proposed model.

To demonstrate the usefulness of the model we conducted a virtual screen to identify potential new active targets within the models domain of applicability threshold. The primary objective of the *in silico* screen was to determine whether the developed *in silico* model could classify structures that are not included in the training or test sets, as active or inactive. The secondary objective was to identify which structural modifications could be tolerated using the domain of applicability. The ultimate role of the *in silico* screen was to be used as a guide to the identification of the most promising new synthetic targets.

During the virtual screening procedure the following chemistry driven small molecules (**1v**–**7v**) have been designed (Fig. 3) in an effort to identify novel potent inhibitors. The design of these molecules builds upon isoxazole framework and previous published paper of our group on rigid pyrazole derivatives (see compounds P 5–8) focusing on the substitution pattern of the two aromatic rings A and B. By this way isoxazoles **1v**–**3v**, **5v**–**7v** were designed. Moreover a pyrazole molecule **4v** was encompassed as a comparison basis molecule with our previous pyrazoles work incorporated in this virtual screening. Isoxazoles **1v** and **2v** differ only in one hydroxyl group that B ring possesses and the model classifies them as actives. Isoxazole **3v** is designed to show the effect of a) protection of hydroxyl group and b) replacement of a hydroxyl group with fluorine atom on the anti-proliferative activity. Although the model classifies this compound as active the experimental validation shows the opposite.

Isoxazole **5v** was designed as an alternative derivative to **2v**. Thus the hydroxyl group (A ring) is replaced by a sulfamic moiety (an electron withdrawing group) while the other two hydroxyl groups were replaced by the fluorine atom. This substitution leads to an inactive compound based on the model. Compound **6v** is a methoxylated analogue of compound **2v** where the tetralonic core of **2v** was substituted by a quinoline moiety. Also this methoxylation leads to an inactive compound (**6v**) based on the model. Replacement of tetralone core to a more flexible one (indanone), provided compound **7v**, in an effort to elucidate effect of change on the rigid skeleton, on the biological activity. Compound **7v** was also predicted as inactive. Compounds **4v**–**7v** that were predicted as inactive were not proposed for experimental investigation.

As mentioned above, among the virtually proposed structures, only three molecules were identified as potentially active inhibitors (**1v**–**3v**) based on the developed model. The structures of these compounds fall within the domain of applicability of the model and were further explored experimentally. These three proposed molecules were synthesized as shown in Schemes 2 and 3 and described in the experimental part. Compounds **15**, **17** and **23** were deprotected almost in quantitative yields to provide compounds **1v**–**3v**. The correlation between C-5, H-7 and H-13 in the HMBC experiment for isoxazoles **1v**–**3v** was used for the unambiguous assignment of the synthesized compounds (see supporting

Fig. 2. Structures of pyrazoles reported in the literature (P1–P8 from Tzanetou et al., 2012 and P9–P16 from Christodoulou et al., 2010).

Table 2
Experimental values and predictions.

Compound ID	Observed class	Predicted class
5	Inactive	Inactive
6	Inactive	Inactive
7	Inactive	Inactive
8[a]	Inactive	Inactive
9	Active	Active
10[a]	Active	Active
11	Active	Active
12	Active	Active
15	Inactive	Inactive
16[a]	Inactive	Inactive
17	Inactive	Inactive
18	Active	Active
19	Active	Active
20[a]	Active	Active
21	Inactive	Inactive
22	Active	Active
23	Active	Active
P1[a]	Inactive	Inactive
P2	Inactive	Inactive
P3	Inactive	Inactive
P4	Inactive	Inactive
P5	Active	Active
P6[a]	Active	Active
P7	Active	Active
P8	Active	Active
P9	Active	Active
P10[a]	Active	Active
P11	Active	Active
P12[a]	Active	Active
P13[a]	Inactive	Active
P14	Active	Active
P15	Active	Active
P16	Active	Active

[a] Compounds included in the test set.

Table 3
Confusion matrix (training set, 10-fold cross validation) random trees.

	Positive predicted	Negative predicted
Positive observed (active)	13	2
Negative observed (inactive)	1	8

information). The results of this *in silico* work were validated as the synthesized compounds were evaluated in four different cell lines as described before. Results are illustrated in Table 6. As seen from the results, two of the proposed compounds, namely compounds **1v** and **2v**, were experimentally verified as actives whereas compound **3v** displayed only moderate or no anti-proliferative activity It is important to highlight the fact that the tri-substituted derivative **2v** displayed the best activity, with IC_{50} values below 1 μM.

Table 4
Confusion matrix (test set) random trees.

	Positive predicted	Negative predicted
Positive observed (active)	5	0
Negative observed (inactive)	1	3

Table 5
Specificity, sensitivity, precision & Accuracy statistics (random trees).

	Specificity	Sensitivity	Precision	Accuracy
Crossvalidation	0.889	0.867	0.929	0.875
External validation	1	0.833	1	0.89

3. Experimental section

3.1. Chemistry

All anhydrous reactions were carried out under argon atmosphere. Solvents were dried by distillation prior to use. Solvent mixtures used in chromatographic separations are reported as volume to volume ratios. Starting materials were purchased from Aldrich as analytical reagent grades and used without further purification. Analytical thin-layer chromatography (TLC) was conducted on Merck glass plates coated with silica gel 60 F_{254} and spots were visualized with UV light or/and an alcohol solution of anisaldehyde. Flash column chromatography was performed using Merck silica gel 60 (230–400 mesh ASTM).

Melting points (Mp) were determined on a Büchi melting point apparatus and are uncorrected. ^{1}H NMR (600 MHz) and ^{13}C NMR (300 MHz) data were recorded on a Bruker Avance 600 spectrometer. COSY, HMQC, and HMBC NMR data were obtained using standard Bruker microprograms. The coupling constants are ^{1}H and ^{15}N NMR recorded in Hertz (Hz) and the chemical shifts are reported in parts per million (δ, ppm), downfield from tetramethylsilane (TMS) that was used as an internal standard.

Infrared spectra were obtained on a Nicolet Magna 750, series II spectrometer. HPLC separations were performed using an Agilent 1100 series instrument with a variable wavelength UV detector and coupled to HP Chem–Station utilizing the manufacturer's 5.01 software package.

3.2. Indicative procedure for the synthesis of isoxazoles

3.2.1. (3,5 Bis(4-methoxyphenyl)isoxazole) (**5**)

4-Methoxyacetophenone (0.5 g, 3.3 mmol) was dissolved in 9 mL of anhydrous toluene, cooled to 0 °C under argon and LiHMDS (3.5 mL, 1.0 M in THF, 3.5 mmol) and added via a syringe in one-pot under stirring. After approximately 1 min to allow the formation of the anion, p-anisoylchloride (0.23 mL, 1.65 mmol) was added. The ice bath was removed and after 1 min 4 mL of AcOH was added. The reaction was stirred for an additional 2 min and consecutively EtOH (17 mL), THF (4 mL) and an excess of hydrochloric hydroxylamine (1.03 g, 15 mmol) were added. The reaction mixture was refluxed for 15 min and completion of the reaction was verified by TLC. Then, the resulting solution was added to 5 mL of 1.0 M NaOH and extracted twice with EtOAc (2 × 20 mL). The combined organic fractions were washed with brine, dried over Na_2SO_4, and evaporated under reduced pressure. The resulting residue was purified by flash column chromatography using a mixture of CH_2Cl_2/n-hexane (9:1) to provide isoxazole **6** (0.75 g, 80%) as white crystalline needles.

^{1}**H NMR** ($CDCl_3$): δ = 3.89 (6H, s, $-OCH_3$), 6.67 (1H, s, H-4), 7.01 (4H, d, *J* 8.5 Hz, H-3′, H-5′, H-3″, H-5″), 7.80 (4H, d, *J* 8.5 Hz, H-2′, H-6′, H-2″, H-6″). ^{13}**C NMR** ($CDCl_3$): δ = 55.3 ($-OCH_3$, $-OCH_3$), 95.8 (C-4), 114.3 (C-3′, C-5′, C-3″, C-5″), 121.0 (C-1′, C-1″), 128.0 (C-2′, C-6′, C-2″, C-6″), 160.9 (C-4′,C-4″), 162.4 (C-3), 169.9 (C-5). Analysis for $C_{17}H_{15}NO_3$: Calculated: C, 72.58; H, 5.37; N, 4.98; Found: C, 72.32; H, 5.30; N, 5.09.

3.2.2. 3,5-Bis-(4-Methoxyphenyl)-4-methylisoxazole (**6**)

This compound was obtained from 1-(4-methoxyphenyl) propan-1-one and p-anisoylchloride as yellow crystalline solid (0.67 g, 76%), using the aforementioned procedure and purified by flash column chromatography (CH_2Cl_2/n-hexane 8.5:1.5).

^{1}H NMR ($CDCl_3$): δ = 1.95 (3H, s, CH_3), 3.89 (6H, s, $-OCH_3$), 7.04 (4H, m, H-3″, H-5″,H-3′, H-5′), 7.64 (2H, d, *J* 9.0 Hz, H-2″, H-6″), 7.71 (2H, d, *J* 9.0 Hz, H-2′, H-6′). Analysis for $C_{18}H_{17}NO_3$: Calculated: C, 73.20; H, 5.80; N, 4.74; Found: C, 73.00; H, 5.94; N, 4.64.

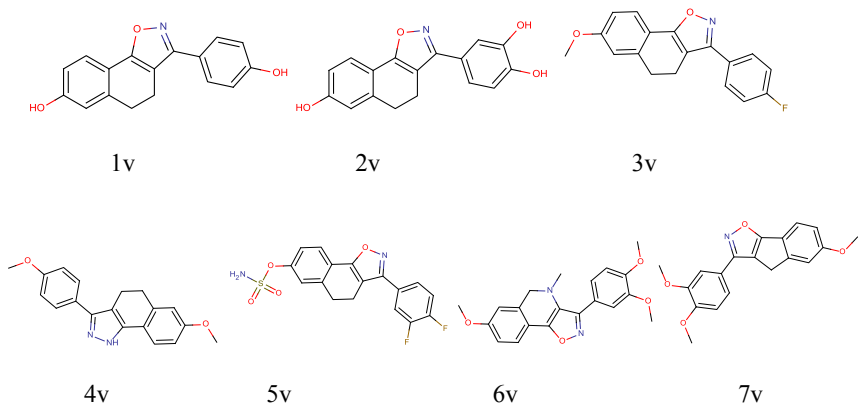

Fig. 3. Chemistry driven virtual screening molecules.

*3.2.3. 4-Ethyl-3,5-bis(4-methoxyphenyl)isoxazole (**7**)*

Reaction of 4-methoxybutyrophenone (0.5 g, 2.8 mmol) with p-anisoylchloride (0.19 mL, 1.4 mmol) using the described procedure provided – after recrystallization from Et_2O – an isoxazole as yellow crystalline solid (0.55 g, 64%).

^{1}H NMR ($CDCl_3$): δ = 1.17 (3H, t, *J* 7.5 Hz, CH_3), 2.73 (2H, q, *J* 7.5 Hz, $-CH_2-$), 3.88 (3H, s, $-OCH_3$), 3.89 (3H, s, $-OCH_3$), 7.35 (4H, m, H-3″, H-5″,H-3′, H-5′), 7.6 (2H, d, *J* 8.5 Hz, H-2″, H-6″), 7.7 (2H, d, *J* 8.5 Hz, H-2′, H-6′). Analysis for $C_{19}H_{19}NO_3$: Calculated: C, 73.77; H, 6.19; N, 4.53; Found: C, 73.97; H, 6.29; N, 4.44.

*3.2.4. 3-(4-Methoxyphenyl)-5-(4-nitrophenyl)-isoxazole (**8**)*

Compound **8** was prepared as a yellow crystalline solid (0.6 g, 75%) following the abovementioned general procedure with 4-nitroacetophenone (0.5 g, 3.0 mmol) and p-anisoylchloride (0.2 mL, 1.5 mmol) substrates and purified by flash column chromatography (CH_2Cl_2/n-hexane 8:2).

^{1}H NMR ($CDCl_3$): δ = 3.92 (3H, s, $-OCH_3$), 6.85 (1H, s, H-4), 7.02 (2H, d, *J* 8.5 Hz, H-3′, H-5′), 8.02 (2H, d, *J* 8.5 Hz, H-2′, H-6′), 8.13 (2H, d, *J* 9.0 Hz, H-2″, H-6″), 8.34 (2H, d, *J* 8.5 Hz, H-3″, H-5″).

Analysis for $C_{16}H_{12}N_2O_4$: Calculated: C, 64.86; H, 4.08; N, 9.46; Found: C, 64.75; H, 4.00; N, 9.50.

*3.2.5. 7-Methoxy-3-(4-methoxyphenyl)-4,5-dihydronaphtho[2,1-d] isoxazole (**15**)*

Compound **15** was synthesized as yellow crystalline solid (0.57 g, 67%), from 6-methoxy-1-tetralone **13** (0.5 g, 2.8 mmol) and p-anisoylchloride (0.19 mL, 1.4 mmol), as previously described, and purified by flash column chromatography (CH_2Cl_2/n-hexane 8.5:1.5).

^{1}**H NMR** ($CDCl_3$): δ = 2.95 (2H, t, *J* 7.5 Hz, H-13), 3.07 (2H, t, *J* 7.5 Hz, H-12), 3.87 (6H, m, $-OCH_3$), 6.86 (1H, dd, *J* 9.0, 2.0 Hz, H-8), 6.88 (1H, d, *J* 2.0 Hz, H-10), 7.02 (2H, d, *J* 8.5 Hz, H-3′, H-5′), 7.67 (1H, d, *J* 9.0 Hz, H-7) 7.72 (2H, d, *J* 8.5 Hz, H-2′, H-6′). ^{13}**C NMR** ($CDCl_3$): δ = 19.4 (C-13), 29.5 (C-12), 55.3 ($-OCH_3$, $-OCH_3$), 108.9 (C-4), 111.8 (C-8), 114.2 (C-10, C-3′, C-5′), 118.7 (C-6), 122.0 (C-1′), 123.4 (C-7), 128.9 (C-2′, C-6′), 138.4 (C-11), 160.0 (C-3), 160.4 (C-9, C-4′), 166.0 (C-5). Analysis for $C_{19}H_{17}NO_3$: Calculated: C, 78.07; H, 5.90; N, 9.10 Found: C, 77.94; H, 5.85; N, 9.21.

Table 6
Experimental results for the proposed compounds.

Compound	IC50 (μM)			
	HMEC-1	MBEC	HeLa	MCF-7
1v	6.7 ± 0.1	4.6 ± 1.7	3.3 ± 0.2	3.1 ± 0.8
2v	0.42 ± 0.12	0.96 ± 0.4	0.97 ± 0.08	0.72 ± 0.14
3v	46 ± 15	38 ± 9	>100	>100

*3.2.6. 7,8-Dimethoxy-3-(4-methoxyphenyl)-4,5-dihydronaphtho [2,1-d]isoxazole (**16**)*

Compound **16** was synthesized as yellow crystalline solid (0.43 g, 51%), according to the previously described procedure, using 6,7-dimethoxy-1-tetralone **14** (0.5 g, 2.5 mmol) and p-anisoylchloride (0.17 mL, 1.25 mmol) substrates and purified by flash column chromatography (CH_2Cl_2/n-hexane 9:1).

^{1}**H NMR** ($CDCl_3$): δ = 2.95 (2H, t, *J* 7.5 Hz, H-13), 3.03 (2H, t, *J* 7.5 Hz, H-12), 3.88 (3H, C-4′-OCH_3), 3.94 (3H, C-9-OCH_3), 3.97 (3H, C-8-OCH_3), 6.83 (1H, s, H-10), 7.02 (2H, d, *J* 8.5 Hz, H-3′, H-5′), 7.67 (1H, d, *J* 9.0 Hz, H-7) 7.72 (2H, d, *J* 8.5 Hz, H-2′, H-6′). ^{13}**C NMR** ($CDCl_3$): δ = 19.7 (C-13), 28.8 (C-12), 55.3 (C-4′-OCH_3), 56.0 (C-9-OCH_3), 56.1 (C-8-OCH_3), 108.8 (C-4), 105.3 (C-7), 111.5 (C-10), 114.2 (C-3′, C-5′), 118.2 (C-6), 122.1 (C-1′), 128.9 (C-2′, C-6′), 129.4 (C-11), 148.1 (C-8), 149.7 (C-9), 159.5 (C-3), 160. 1 (C-4′), 166.3 (C-5). Analysis for $C_{20}H_{19}NO_4$: Calculated: C, 71.20; H, 5.68; N, 4.15; Found C, 71.30; H, 5.75; N, 4.18.

*3.2.7. 3-(3,4-Dimethoxyphenyl)-7-methoxy-4,5-dihydronaphtho [2,1-d]isoxazole, (**17**)*

Compound **17** was obtained as a yellow crystalline solid (0.65 g, 67%) from 6-methoxy-1-tetralone **13** (0.5 g, 2.8 mmol) and dimethoxybenzoyl chloride (0.23 mL, 1.4 mmol) substrates and purified by flash column chromatography (CH_2Cl_2/n-hexane 9:1).

^{1}**H NMR** ($CDCl_3$): δ = 2.98 (2H, t, *J* 7.5 Hz, H-13), 3.07 (2H, t, *J* 7.5 Hz, H-12), 3.86 (3H, C-4′-OCH_3), 3.95 (3H, C-9-OCH_3), 3.97 (3H, C-8-OCH_3), 6.86 (2H, m, H-8, H-10), 6.97 (1H, d, *J* 8.5 Hz H-5′), 7.27 (1H, s, H-7), 7.4 (1H, s, H-6′), 7.67 (1H, d, *J* 9.5 Hz H-2′). Analysis for $C_{20}H_{19}NO_4$: Calculated: C, 71.20; H, 5.68; N, 4.15; Found C, 71.37; H, 5.77; N, 4.21.

*3.2.8. 3-(3,4-Dimethoxyphenyl)-7,8-dimethoxy-4,5-dihydronaphtho[2,1-d]isoxazole (**18**)*

Compound **18** was synthesized according to the abovementioned procedure for the synthesis of isoxazoles using 6,7-dimethoxy-1-tetralone **14** (0.5 g, 2.5 mmol) and dimethoxybenzoyl chloride (0.21 mL, 1.25 mmol) as reactants. Recrystallization from Et_2O provided **18** (0.58 g, 63%) as pale-yellow crystals.

^{1}**H NMR** ($CDCl_3$): δ = 2.97 (2H, t, *J* 7.5 Hz, H-13), 3.05 (2H, t, *J* 7.5 Hz, H-12), 3.95 (3H, C-4′-OCH_3), 3.96 (3H, C-9-OCH_3), 3.98 (6H, m, C-8-OCH_3, C-3′-OCH_3), 6.85 (1H, s, H-10), 6.99 (1H, d, *J* 8.5 Hz, H-5′), 7.27 (1H, s, H-7), 7.28 (1H, dd, *J* 8.5, 2.0 Hz, H-6′), 7.39 (1H, d, *J* 1.8 Hz, H-2′).

^{13}C NMR ($CDCl_3$): δ = 19.7 (C-13), 28.9 (C-12), 56.0 (−OCH_3, −OCH_3, −OCH_3, −OCH_3), 108.8 (C-4), 105.3 (C-7), 110.4 (C-2′), 110.9 (C-5′), 111.4 (C-10), 117.9 (C-6), 120.4 (C-6′), 122.2 (C-1′), 129.0 (C-11), 148.1 (C-8), 149.0 (C-3′), 149.6 (C-4′), 150.0 (C-9), 159.5 (C-3), 166.4 (C-5).

Analysis for $C_{21}H_{21}NO_5$: Calculated: C, 68.65; H, 5.76; N, 3.81; Found C, 68.77; H, 5.81; N, 3.91.

3.2.9. 7-Methoxy-3-(4-(trifluoromethylthio)phenyl)-4,5-dihydronaphtho[2,1-d]isoxazole (**21**)

Compound **23** was synthesized as pale brown crystalline solid (0.52 g, 49%) from 6-methoxy-1-tetralone **13** (0.5 g, 2.8 mmol) and 4-(trifluoromethylthio)benzoyl chloride (0.24 mL, 1.4 mmol) substrates in accordance with the general procedure for the synthesis of isoxazoles and purified by flash column chromatography (CH_2Cl_2/n-hexane 8.5:1.5).

^{1}H NMR ($CDCl_3$): δ = 2.98 (2H, t, H-13), 3.09 (2H, t, H-12), 3.87 (3H, −OCH_3), 6.87 (1H, d, *J* 2 Hz, H-10), 6.88 (1H, dd, *J* 8.5, 2.0 Hz, H-8), 7.68 (1H, d, *J* 8.5 Hz, H-7), 7.79 (2H, dd, *J* 8.5, 2.0 Hz, H-3′, H-5′), 7.84 (2H, dd, *J* 8.5, 2.0 Hz, H-2′, H-6′). **^{13}C NMR** ($CDCl_3$): δ = 19.7 (C-13), 28.9 (C-12), 56.0 (−OCH_3) 108.8 (C-4), 112.0 (C-8), 114.4 (C-10), 118.2 (C-6), 123.6 (C-7), 128.4 (C-2′, C-6′), 132.2 (C-1′), 136.6 (C-3′, C-4′ C-5′), 138.2 (C-11), 158.8 (C-3), 160.9 (C-9), 167.1 (C-5).

$C_{19}H_{14}F_3NO_2S$: Calculated: C, 60.47; H, 3.74; N, 3.71 Found: C, 60.59; H, 3.84; N, 3.81.

3.2.10. 3-(4-Fluorophenyl)-7-methoxy-4,5-dihydronaphtho[2,1-d] isoxazole, (**23**)

Compound **25** was synthesized with respect to the above-mentioned procedure for the synthesis of isoxazoles using 6-methoxy-1-tetralone **13** (0.5 g, 2.8 mmol) and 4-fluorobenzoyl chloride (0.17 mL, 1.4 mmol) as reactants. Purification by flash column chromatography (CH_2Cl_2/n-hexane 8:2) provided (0.52 g, 63%) a pale yellow crystalline solid.

^{1}H NMR ($CDCl_3$): δ = 2.98 (2H, t, H-13), 3.09 (2H, t, H-12), 3.87 (3H, −OCH_3), 6.87 (1H, d, *J* 2 Hz, H-10), 6.88 (1H, dd, *J* 8.5, 2.0 Hz, H-8), 7.68 (1H, d, *J* 8.5 Hz, H-7), 7.79 (2H, dd, *J* 8.5, 2.0 Hz, H-3′, H-5′), 7.84 (2H, dd, *J* 8.5, 2.0 Hz, H-2′, H-6′).

$C_{18}H_{14}FNO_2$: Calculated: C, 73.21; H, 4.78; N, 4.74; Found C, 73.31; H, 4.88; N, 4.79.

3.3. Indicative procedure for the demethylation of isoxazoles

3.3.1. 4,4′-(Isoxazole-3,5-diyl)diphenol (**9**)

This compound was obtained as pale yellow crystalline solid (yield, 88%), by demethylation of isoxazole **5**, in accordance with the previously described procedure.

^{1}H NMR (CD_3OD): δ = 6.92 (2H, d, *J* 8.5 Hz, H-3″, H-5″), 6.96 (2H, H-3′, H-5′), 7.33 (1H, s, H-4), 7.48 (2H, *J* 8.5, H-2″, H-6″), 7.62 (2H, d, *J* 8.5 Hz, H-2′, H-6′). **^{13}C NMR** (CD_3OD): δ = 9.0 (CH_3), 98.4 (C-4), 115.6 (C-3′, C-5′, C-3″, C-5″), 121.1 (C-1′, C-1″), 129.2 (C-2′, C-6′), 130.4 (C-2″, C-6″), 160.2 (C-4′, C-4″), 164.9 (C-3), 166.5 (C-5). Analysis for $C_{15}H_{11}NO_3$: Calculated: C, 71.14; H, 4.38; N, 5.24; Found: C, 71.24; H, 4.29; N, 5.32.

3.3.2. 4,4′-(4-Methylisoxazole-3,5-diyl)diphenol (**10**)

To a stirred solution of isoxazole **6** (0.1 g, 0.34 mmol) in CH_2Cl_2 (15 mL), cooled at −78 °C, BBr_3 (4.74 mmol, 1.0 M in CH_2Cl_2, 5 equiv per bond, 4.74 mL) was added dropwise. The reaction was stirred for 1 h at −78 °C and 17 h at ambient temperature. Then, the reaction was placed in an ice-bath, quenched with MeOH and water (10 mL) and HCl 1N (3–4 drops) was added to neutralize the pH. The organic layer was obtained by extraction with EtOAc (2 × 15 mL). The combined organic extracts were washed with water, brine, dried over Na_2SO_4, filtered and evaporated under reduced pressure. The product was purified with flash column chromatography (n-Hexane/EtOAc 4:6) or recrystallized from Et_2O resulting in a yellow crystalline solid (87% yield).

^{1}H NMR (CD_3OD): δ = 2.27 (3H, CH_3), 6.95 (2H, d, *J* 8.5 Hz, H-3″, H-5″), 6.96 (2H, H-3′, H-5′), 7.51 (2H, J 8.5, H-2″, H-6″), 7.62 (2H, d, *J* 8.5 Hz, H-2′, H-6′). **^{13}C NMR** (CD_3OD): δ = 9.0 (CH_3), 107.4 (C-4), 116.2 (C-3′, C-5′, C-3″, C-5″), 120.7 (C-1′, C-1″), 129.3 (C-2′, C-6′), 130.4 (C-2″, C-6″), 160.0 (C-4′, C-4″), 164.9 (C-3), 167.0 (C-5). Analysis for $C_{16}H_{13}NO_3$: Calculated: C, 71.90; H, 4.90; N, 5.24; Found: C, 71.80; H, 4.83; N, 5.18.

3.3.3. 4,4′-(4-Ethylisoxazole-3,5-diyl)diphenol (**11**)

This compound was obtained from isoxazole **7** as yellow crystalline solid, in accordance with the previously described procedure (yield, 90%).

^{1}H NMR (Acetone-d6): δ = 1.16 (3H, t, *J* 7.5 Hz, CH_3), 2.79 (2H, q, *J* 7.5 Hz, −CH_2−), 7.05 (2H, d, *J* 8.5 Hz, H-3″, H-5″), 7.08 (2H, d, *J* 8.5, H-3′, H-5′), 7.59 (2H, d, *J* 8.5 Hz, H-2″, H-6″) 7.68 (2H, d, *J* 8.5, H-2′, H-6′). **^{13}C NMR** (Acetone-d6): δ = 13.6 (−CH_2), 15.6 (−CH_2−), 115.5 (C-3″, C-5″), 115.7 (C-3′, C-5′), 119.7 (C-1′), 121.2 (C-1″), 128.3 (C-2′, C-6′), 129.5 (C-2″, C-6″), 158.2 (C-4′, C-4″), 162.7 (C-3), 165.1 (C-5). Analysis for $C_{15}H_{11}NO_3$: Calculated: C, 72.58; H, 5.37; N, 4.98; Found: C, 72.44; H, 5.29; N, 4.92.

3.3.4. 4-(5-(4-Nitrophenyl)isoxazol-3-yl)phenol (**12**)

This compound was obtained from nitrophenyl isoxazole **8** as yellow crystalline solid, in accordance with the previously described procedure (yield, 95%).

^{1}H NMR (Acetone): δ = 7.01 (2H, d, *J* 8.5 Hz, H-3′, H-5′), 7.33 (1H, s, H-4), 7.82 (2H, d, *J* 8.5 Hz, H-2′, H-6′), 8.23 (2H, J 8.5, H-2″, H-6″) 8.40 (2H, H-3″, H-5″). **^{13}C NMR** (Acetone): δ = 97.0 (C-4), 116.6 (C-3′, C-5′), 124.8 (C-3″, C-5″), 128.2 (C-2′, C-6′), 128.6 (C-2″, C-6″), 120.4 (C-1′), 137.2 (C-1″), 150.3 (C-4″), 161.2 (C-4′), 162.3 (C-3), 173.2 (C-5). Analysis for $C_{15}H_{10}N_2O_4$: Calculated: C, 63.83; H, 3.57; N, 9.92; Found: C, 63.94; H, 3.49; N, 10.01.

3.3.5. 3-(4-Hydroxyphenyl)-4,5-dihydronaphtho[2,1-d]isoxazol-7-ol (**1v**)

This compound was obtained by demethylation from isoxazole **15** as a pale green crystalline solid, according to the general deprotection procedure (yield, 92%).

^{1}H NMR (DMSO): δ = 2.84 (2H, t, *J* 7.4 Hz, H-13), 2.96 (2H, t, *J* 7.4 Hz, H-12), 6.70 (1H, dd, *J* 8.5, 2.0 Hz H-8), 6.79 (1H, d, *J* 2.0 Hz H-10), 6.95 (2H, d, *J* 8.5 Hz, H-3′, H-5′), 7.51 (2H, J 8.5 Hz, H-2′, H-6′), 7.48 (1H, d, *J* 8.5 Hz, H-7).

^{13}C NMR (DMSO): δ = 18.9 (C-13), 28.5 (C-12), 108.7 (C-4), 113.3 (C-8), 114.2 (C-2′), 115.3 (C-10), 115.7 (C-5′), 116.3 (C-6), 117.4 (C-3′) 118.7 (C-6′), 120.7 (C-1′), 122.7 (C-7), 146.2 (C-4′), 159.4 (C-3), 159.7 (C-9), 166.3 (C-5).

Analysis for $C_{17}H_{13}NO_3$: Calculated: C, 73.11; H, 4.69; N, 5.02; Found C, 72.97; H, 4.58; N, 4.91.

3.3.6. 3-(4-Hydroxyphenyl)-4,5-dihydronaphtho[2,1-d]isoxazole-7,8-diol (**19**)

This compound was obtained from isoxazole **16** as pale yellow crystalline solid, in accordance with the general deprotection procedure (yield, 89%).

^{1}H NMR (DMSO): δ = 2.85 (2H, t, *J* 7.4 Hz, H-13), 2.96 (2H, t, *J* 7.4 Hz, H-12), 6.90 (1H, d, *J* 2.1 Hz H-10), 6.95 (2H, d, *J* 8.5 Hz, H-3′, H-5′), 7.48 (1H, s, H-7), 7.53 (2H, *J* 8.5 Hz, H-2′, H-6′).

Analysis for $C_{17}H_{13}NO_4$: Calculated: C, 69.15; H, 4.44; N, 4.74; Found C, 69.30; H, 4.37; N, 4.69.

*3.3.7. 4-(7-Hydroxy-4,5-dihydronaphtho[2,1-d]isoxazol-3-yl) benzene-1,2-diol (**2v**)*

This compound was prepared from isoxazole **17** as pale yellow crystalline solid, following the general deprotection procedure (yield, 92%).

^{1}**H NMR** (DMSO): $\delta = 2.85$ (2H, t, H-13), 2.96 (2H, t, H-12), 6.73 (1H, dd, *J* 8.5, 2.0 Hz H-8), 6.78 (1H, d, *J* 2.0 Hz H-10), 6.85 (1H, d, *J* 8.5 Hz, H-5′), 7.03 (1H, dd, *J* 8.5, 2.0 Hz, H-6′), 7.18 (1H, d, *J* 2.0 Hz, H-2′), 7.45 (1H, d, *J* 8.5 Hz, H-7). ^{13}**C NMR** (DMSO): $\delta = 18.6$ (C-13), 28.4 (C-12), 108.7 (C-4), 113.5 (C-8), 114.2 (C-2′), 115.3 (C-10), 115.7 (C-5′), 116.3 (C-6), 118.7 (C-6′), 120.7 (C-1′), 122.7 (C-7), 138.6 (C-11), 146.2 (C-4′), 159.4 (C-3′), 159.4 (C-3), 159.5 (C-9), 165.6 (C-5). $C_{17}H_{13}NO_4$: Calculated: C, 69.15; H, 4.44; N, 4.74; Found: C, 69.25; H, 4.39; N, 4.67.

*3.3.8. 3-(3,4-Dihydroxyphenyl)-4,5-dihydronaphtho[2,1-d] isoxazole-7,8-diol (**20**)*

This compound was obtained from isoxazole **18** as pale yellow crystalline solid, following the general deprotection procedure (yield, 93%).

^{1}**H NMR** (DMSO): $\delta = 2.84$ (2H, t, *J* 7.4 Hz, H-13), 2.96 (2H, t, *J* 7.4 Hz, H-12), 6.87 (1H, d, *J* 8.5 Hz, H-5′), 6.90 (1H, d, *J* 2.1 Hz H-10), 7.03 (1H, dd, *J* 8.5, 2.0 Hz, H-6′), 7.18 (1H, d, *J* 2.0 Hz, H-2′), 7.48 (1H, s, H-7).

$C_{17}H_{13}NO_5$: Calculated: C, 65.59; H, 4.21; N, 4.50; Found: C, 65.50; H, 4.19; N, 4.47.

*3.3.9. 3-(4-(Trifluoromethylthio)phenyl)-4,5-dihydronaphtho[2,1-d]isoxazol-7-ol, (**22**)*

This compound was obtained from isoxazole **23** (0.1 g, 0.26 mmol), as pale green crystalline solid following the general deprotection procedure (0.09 g, yield 94%).

^{1}**H NMR** (Acetone-d6): $\delta = 3.01$ (2H, t, *J* 7.4 Hz, H-13), 3.07 (2H, t, *J* 7.4 Hz, H-12), 6.87 (2H, m, ArH), 7.56 (1H, d, *J* 8.0 Hz, ArH), 7.90 (2H, d, *J* 8.0 Hz, ArH), 7.98 (2H, d, *J* 8.5 Hz, ArH).

$C_{19}H_{14}F_3NO_2S$: Calculated: C, 60.47; H, 3.74; N, 3.71 Found: C, 60.59; H, 3.84; N, 3.81.

*3.3.10. 3-(4-Fluorophenyl)-4,5-dihydronaphtho[2,1-d]isoxazol-7-ol (**3v**)*

This compound was obtained from isoxazole **25** as pale yellow crystalline solid, following the general deprotection procedure (yield, 94%).

^{1}**H NMR** (CD_3OD): $\delta = 2.93$ (2H, t, H-13), 3.05 (2H, t, H-12), 6.78 (1H, dd, *J* 8.5, 2.0 Hz H-8), 6.81 (1H, d, *J* 2.0 Hz H-10), 7.29 (2H, d, *J* 8.5 Hz, H-3′, H-5′), 7.53 (1H, d, *J* 8.5, Hz, H-7), 7.80 (2H, dd, *J* 8.5, 2.0 Hz, H-2′, H-6′). ^{13}**C NMR** (CD_3OD): $\delta = 18.7$ (C-13), 28.8 (C-12), 108.7 (C-4), 113.6 (C-8), 115.6/115.1 (C-3′, C-5′), 115.1 (C-10), 116.6 (C-6), 122.9/129.3 (C-2′, C-6′), 125.8 (C-1′), 159.2 (C-3), 159.5(C-9), 164.1 (C-4′), 166.4 (C-5).

$C_{17}H_{12}FNO_2$: Calculated: C, 72.59; H, 4.30; N, 4.98; Found C, 72.74; H, 4.23; N, 4.89.

3.4. Biological part

3.4.1. Cell cultures

Mouse brain endothelial cells (MBEC) were provided by Prof. M. Presta (Brescia, Italy). Human cervical carcinoma (Hela) and human breast carcinoma (MCF-7) cells were obtained from the American Type Culture Collection (ATCC, Middlesex, UK). The cells were grown in Dulbecco's modified minimum essential medium (DMEM, Life Technologies, Inc., Rockville, MD) supplemented with 10 mM Hepes (Life Technologies, Inc., Rockville, MD) and 10% fetal bovine serum (FBS, Harlan Sera-Lab Ltd., Loughborough, UK). Human microvascular endothelial cells (HMEC-1) were obtained from the CDC (Atlanta, USA) and grown in EGM-2 MV BulletKit endothelial cell medium (Lonza, Verviers, Belgium).

3.4.2. Cell proliferation assays

Cells were seeded in 48-well plates at 10,000 cells per cm^2. After 16 h, the cells were incubated in fresh medium in the presence of 5-fold dilutions of the test compounds. On day 5, cells were trypsinized and counted by a Coulter counter (Analis, Belgium). The compound concentration that inhibits cell growth by 50% (i.e. IC_{50}) was calculated based on cell counts in control cultures.

3.5. Computational part

3.5.1. Molecular descriptors - separation into a training and a test set

For each compound we calculated a large number of descriptors that account for their chemical, physicochemical, electronic and quantum characteristics. Following the optimization of the compound geometries using the PM6 method included in MOPAC2009 [J.J.P. Stewart, J. Mol. Model. 13 (2007) 1173–1213, J.J.P. Stewart, J. Mol. Model. 14 (2008) 499–535], the descriptors were calculated using the Chemistry Development Kit (CDK) [20]. The PM6 method was chosen for the geometry optimizations since it offered a good balance between speed and accuracy. A recent paper highlighted the quality of models obtained by the PM6 method as similar to that of models based on B3LYP32 (Density Functional Theory) [29]. After the optimization, 294 input attributes were calculated for each compound including topological, structural, electronic and physicochemical descriptors. The Hela inhibition data along with the corresponding full set of descriptor values were used in the variable selection procedure.

3.5.2. Variable selection

Variable selection techniques have become an apparent need in many chemoinformatics applications and different methods have been successfully applied as variable selection tools in QSAR problems. As some of the descriptors do not have any discrimination power (i.e. they have no variation) a filter was applied for their removal. In total 159 descriptors remained to be used as possible inputs during the QSAR model development. Before running the classification methodology, the most significant attributes among the 159 available were preselected by using CfsSubset variable selection and BestFirst evaluator, which are included in Weka [25]. Correlation-based feature subset selection (CfsSubset) algorithm evaluated the value of a subset of attributes by considering the individual predictive ability of each feature along with the degree of redundancy between them. Subsets of features that were highly correlated with the class while having low intercorrelation were preferred.

3.5.3. Modeling methods

Random forest is a machine learning method that consists of many decision trees and outputs a prediction combining the result given from the individual trees [Leo Breiman (2001). Random Forests. Machine Learning. 45(1):5–32.]. Individual random trees are grown based on samples from the original dataset. These samples are used to construct training sets and build trees. A random number of attributes are chosen for each tree. These attributes form the nodes and leafs of the tree. In this work, the implementation of the random forest algorithm available in WEKA [25] was used including 4 variables for the model development. Predictions were made by averaging predicted activities over all trees in the final forest.

3.5.4. Model validation

The internal performance, as represented by goodness-of-fit and robustness, and the predictivity of a model, as determined by external validation, needs to be evaluated. The produced model was validated using external validation (Tropsha, 2010). The model was internally and externally validated paying special attention to the principles of model validation for accepting QSAR models as described by the Organisation for Economic Cooperation and Development (OECD).

The validation of the proposed model was assessed by various validation techniques. In particular the proposed classification models were fully validated using the following measurements:

$$\text{Precision} = \frac{TP}{TP + FP} \quad (1)$$

$$\text{Sensitivity} = \frac{TP}{TP + FN} \quad (2)$$

$$\text{Specificity} = \frac{TN}{TN + FP} \quad (3)$$

$$\text{Accuracy} = \frac{TP + TN}{TP + FP + FN + TN} \quad (4)$$

where: TP = True Positive, FP = False Positive, TN = True Negative, FN = False Negative.

Confusion Matrix is also given as shown below:

	Positive predicted	Negative predicted
Positive observed (active)	TP	FN
Negative observed (inactive)	FP	TN

External validation was applied, by randomly splitting the dataset into training and validation set in a proportion of 70:30. The separation of the dataset was performed using the Partitioning KNIME node by applying the default random seed. The use of random seed provides reproducible results upon re-execution of the node. The 10 compounds that constituted the test set were not involved by any means in the training procedure.

3.5.5. Applicability domain

In order for an *in silico* model to be used for screening new compounds, its domain of application must be defined and predictions for only those compounds that fall into this domain may be considered reliable. Similarity measurements were used to define the domain of applicability of the two models based on the Euclidean distances among all training compounds and the test compounds. The distance of a test compound to its nearest neighbor in the training set was compared to the predefined applicability domain (APD) threshold. The prediction was considered unreliable when the distance was higher than APD. APD was calculated as follows:

$$\text{APD} = < d > + Z\sigma \quad (6)$$

Calculation of $<d>$ and σ was performed as follows: First, the average of Euclidean distances between all pairs of training compounds was calculated. Next, the set of distances that were lower than the average was formulated. $<d>$ and σ were finally calculated as the average and standard deviation of all distances included in this set. Z was an empirical cutoff value and for this work, it was chosen equal to 0.5. The calculation of the domain of applicability was done using Enalos KNIME nodes [http://www.novamechanics.com/knime.php].

4. Conclusions

A series of novel isoxazole derivatives were synthesized by a simple procedure based on a modification of a methodology published in 2006 for the *in situ* synthesis of pyrazoles, adapted for isoxazoles. All compounds were tested in four different cell lines to evaluate their antiproliferative activity. Based on the Hela cells results of this study and our previous work, a classification model to predict the anti-proliferative activity of isoxazole and pyrazole derivatives was developed. After the calculation of a large number of descriptors, we selected for each compound the most significant descriptors that fully describe the characteristics responsible for the inhibitory activity under study. Based on this dataset, we used Random Forest modeling which resulted in the development of an accurate and reliable model that was fully validated using various cross-validation and external test prediction techniques. A virtual screening study was then proposed for the design of novel active derivatives. In this scenario, the classification model was used to screen out inactive compounds, while the applicability domain served as a valuable tool to filter out “dissimilar” combinations. Overall, compounds 9 and 11 demonstrated significant cytostatic activity, the fused isoxazole derivative 18 and the virtually proposed compound **2v**, were proved at least 10 times more potent than 9, with IC50 values near and below 1 μM. In conclusion a new series of isoxazole compounds was exploited with some of them exhibiting promising cytostatic activities. Further studies on the substitution pattern of the isoxazole core can potentially provide compounds with cytostatic action at the nM scale. In this direction the *in silico* approach described can also be used to screen existing databases [or virtual combinations] to identify derivatives with desired activity.

Acknowledgments

The authors wish to thank Eef Meyen for excellent technical assistance. S.A.H., A.A. and G.M. acknowledge support from Cost Action CM1106 “Chemical Approaches to Targeting Drug Resistance in Cancer Stem Cells” (2012–2015).

Appendix A. Supplementary data

Supplementary data related to this article can be found at http://dx.doi.org/10.1016/j.ejmech.2014.05.011.

References

[1] S. Liekens, A. Bronckaers, M. Belleri, A. Bugatti, R. Sienaert, D. Ribatti, B. Nico, A. Gigante, E. Casanova, G. Opdenakker, M.J. Perez-Perez, J. Balzarini, M. Presta, The thymidine phosphorylase inhibitor 5′-O-tritylinosine (KIN59) is an anti-angiogenic multitarget fibroblast growth factor-2 antagonist, Mol. Cancer Ther. 11 (2012) 817–829.
[2] D. Hanahan, R.A. Weinberg, Hallmarks of cancer: the next generation, Cell 144 (2011) 646–674.
[3] K.M. Cheung, T.P. Matthews, K. James, M.G. Rowlands, K.J. Boxall, S.Y. Sharp, A. Maloney, S.M. Roe, C. Prodromou, L.H. Pearl, G.W. Aherne, E. McDonald, P. Workman, The identification, synthesis, protein crystal structure and in vitro biochemical evaluation of a new 3,4-diarylpyrazole class of Hsp90 inhibitors, Bioorg. Med. Chem. Lett. 15 (2005) 3338–3343.
[4] C. Wasylyk, H. Zheng, C. Castell, L. Debussche, M.C. Multon, B. Wasylyk, Inhibition of the ras-net (Elk-3) pathway by a novel pyrazole that affects microtubules, Cancer Res. 68 (2008) 1275–1283.
[5] C. Didelot, D. Lanneau, M. Brunet, A.L. Joly, A. De Thonel, G. Chiosis, C. Garrido, Anti-cancer therapeutic approaches based on intracellular and extracellular heat shock proteins, Curr. Med. Chem. 14 (2007) 2839–2847.

[6] T. Taldone, A. Gozman, R. Maharaj, G. Chiosis, Targeting Hsp90: small-molecule inhibitors and their clinical development, Curr. Opin. Pharmacol. 8 (2008) 370–374.
[7] S.A. Eccles, A. Massey, F.I. Raynaud, S.Y. Sharp, G. Box, M. Valenti, L. Patterson, A.D. Brandon, S. Gowan, F. Boxall, W. Aherne, M. Rowlands, A. Hayes, V. Martins, F. Urban, K. Boxall, C. Prodromou, L. Pearl, K. James, T.P. Matthews, K.M. Cheung, A. Kalusa, K. Jones, E. McDonald, X. Barril, P.A. Brough, J.E. Cansfield, B. Dymock, M.J. Drysdale, H. Finch, R. Howes, R.E. Hubbard, A. Surgenor, P. Webb, M. Wood, L. Wright, P. Workman, NVP-AUY922: a novel heat shock protein 90 inhibitor active against xenograft tumor growth, angiogenesis, and metastasis, Cancer Res. 68 (2008) 2850–2860.
[8] M.R. Jensen, J. Schoepfer, T. Radimerski, A. Massey, C.T. Guy, J. Brueggen, C. Quadt, A. Buckler, R. Cozens, M.J. Drysdale, C. Garcia-Echeverria, P. Chene, NVP-AUY922: a small molecule HSP90 inhibitor with potent antitumor activity in preclinical breast cancer models, Breast Cancer Res. 10 (2008) R33.
[9] P.A. Brough, W. Aherne, X. Barril, J. Borgognoni, K. Boxall, J.E. Cansfield, K.M.J. Cheung, I. Collins, N.G.M. Davies, M.J. Drysdale, B. Dymock, S.A. Eccles, H. Finch, A. Fink, A. Hayes, R. Howes, R.E. Hubbard, K. James, A.M. Jordan, A. Lockie, V. Martins, A. Massey, T.P. Matthews, E. McDonald, C.J. Northfield, L.H. Pearl, C. Prodromou, S. Ray, F.I. Raynaud, S.D. Roughley, S.Y. Sharp, A. Surgenor, D.L. Walmsley, P. Webb, M. Wood, P. Workman, L. Wrightt, 4,5-diarylisoxazole HSP90 chaperone inhibitors: potential therapeutic agents for the treatment of cancer, J. Med. Chem. 51 (2008) 196–218.
[10] A. Kamal, J.S. Reddy, M.J. Ramaiah, D. Dastagiri, E.V. Bharathi, M.A. Azhar, F. Sultana, S.N.C.V.L. Pushpavalli, M. Pal-Bhadra, A. Juvekar, S. Sen, S. Zingde, Design, synthesis and biological evaluation of 3,5-diaryl-isoxazoline/isoxazole-pyrrolobenzodiazepine conjugates as potential anticancer agents, Eur. J. Med. Chem. 45 (2010) 3924–3937.
[11] D. Simoni, M. Roberti, F.P. Invidiata, R. Rondanin, R. Baruchello, C. Malagutti, A. Mazzali, M. Rossi, S. Grimaudo, F. Capone, L. Dusonchet, M. Meli, M.V. Raimondi, M. Landino, N. D'Alessandro, M. Tolomeo, D. Arindam, S. Lu, D.M. Benbrook, Heterocycle-containing retinoids. Discovery of a novel isoxazole arotinoid possessing potent apoptotic activity in multidrug and drug-induced apoptosis-resistant cells, J. Med. Chem. 44 (2001) 2308–2318.
[12] M.S. Christodoulou, S. Liekens, K.M. Kasiotis, S.A. Haroutounian, Novel pyrazole derivatives: synthesis and evaluation of anti-angiogenic activity, Bioorg. Med. Chem. 18 (2010) 4338–4350.
[13] E. Tzanetou, S. Liekens, K.M. Kasiotis, N. Fokialakis, S.A. Haroutounian, Novel pyrazole and indazole derivatives: synthesis and evaluation of their anti-proliferative and anti-angiogenic activities, Arch. Pharm. 345 (2012) 804–811.
[14] A.A. Toropov, A.P. Toropova, E. Benfenati, QSAR-modeling of toxicity of organometallic compounds by means of the balance of correlations for InChI-based optimal descriptors, Mol. Divers 14 (2010) 183–192.
[15] V.D. Mouchlis, G. Melagraki, T. Mavromoustakos, G. Kollias, A. Afantitis, Molecular modeling on pyrimidine-urea inhibitors of TNF-alpha production: an integrated approach using a combination of molecular docking, classification techniques, and 3D-QSAR CoMSIA, J. Chem. Inf. Model 52 (2012) 711–723.
[16] S. Deswal, N. Roy, A novel range based QSAR study of human neuropeptide Y (NPY) Y5 receptor inhibitors, Eur. J. Med. Chem. 42 (2007) 463–470.
[17] M.S.M. Ahmed, K. Kobayashi, A. Mori, One-pot construction of pyrazoles and isoxazoles with palladium-catalyzed four-component coupling, Org. Lett. 7 (2005) 4487–4489.
[18] S.T. Heller, S.R. Natarajan, 1,3-Diketones from acid chlorides and ketones: a rapid and general one-pot synthesis of pyrazoles, Org. Lett. 8 (2006) 2675–2678.
[19] G. Melagraki, A. Afantitis, Enalos KNIME nodes: exploring corrosion inhibition of steel in acidic medium, Chemometr. Intell. Lab 123 (2013) 9–14.
[20] C. Steinbeck, Y.Q. Han, S. Kuhn, O. Horlacher, E. Luttmann, E. Willighagen, The chemistry development kit (CDK): an open-source java library for chemo- and bioinformatics, J. Chem. Inf. Comp. Sci. 43 (2003) 493–500.
[21] R.S. Pearlman, K.M. Smith, Metric validation and the receptor-relevant subspace concept, J. Chem. Inf. Comp. Sci. 39 (1999) 28–35.
[22] F.R. Burden, A chemically intuitive molecular index based on the eigenvalues of a modified adjacency matrix, Quant. Struct. Act Rel. 16 (1997) 309–314.
[23] R. Todeschini, P. Gramatica, New 3D molecular descriptors: the WHIM theory and QAR applications, Perspect. Drug Discov. Des. (1998) 355–380.
[24] R. Todeschini, V. Consonni, in: H. Kubinyi, R. Mannhold, G. Folkers (Eds.), Molecular Descriptors for Chemoinformatics, Wiley – VCH, Weinheim, 2009.
[25] M. Hall, E. Frank, G. Holmes, B. Pfahringer, P. Reutemann, I.H. Witten, The WEKA data mining software: an update, SIGKDD Explor. Newsl. 11 (2009) 10–18.
[26] G. Melagraki, A. Afantitis, H. Sarimveis, O. Igglessi-Markopoulou, P.A. Koutentis, G. Kollias, In silico exploration for identifying structure-activity relationship of MEK inhibition and oral bioavailability for isothiazole derivatives, Chem. Biol. Drug Des. 76 (2010) 397–406.
[27] G. Melagraki, A. Afantitis, H. Sarimveis, P.A. Koutentis, J. Markopoulos, O. Igglessi-Markopoulou, Identification of a series of novel derivatives as potent HCV inhibitors by a ligand-based virtual screening optimized procedure, Bioorg. Med. Chem. 15 (2007) 7237–7247.
[28] A. Afantitis, G. Melagraki, H. Sarimveis, P.A. Koutentis, J. Markopoulos, O. Igglessi-Markopoulou, Development and evaluation of a QSPR model for the prediction of diamagnetic susceptibility, Qsar. Comb. Sci. 27 (2008) 432–436.
[29] T. Puzyn, N. Suzuki, M. Haranczyk, J. Rak, Calculation of quantum-mechanical descriptors for QSPR at the DFT level: is it necessary? J. Chem. Inf. Model 48 (2008) 1174–1180.